Enhanced CO_2 electrolysis with $SrTiO_3$ cathode through dual doping strategy

Lingting Ye, [a,b] Xiuli Hu, [a,b] Xin Wang, [a] Fanglin Chen,[c] Dian Tang, [a,*] Dehua Dong, [d,*] Kui Xie [b,*]

[a] College of Materials Science and Engineering, Fuzhou University, Xueyuan Road No. 2, Fuzhou, Fujian 350116, China.

[b] CAS Key Laboratory of Design and Assembly of Functional Nanostructures, and Fujian Provincial Key Lab of Nanomaterials, Fujian Institute of Research on the Structure of Matter, Chinese Academy of Sciences, Fuzhou, Fujian 350002, China.

[c] Department of Mechanical Engineering, University of South Carolina, 300 Main Street, Columbia, SC 29208, USA.

[d] School of Material Science and Engineering, University of Jinan, Jinan, Shandong 250022, China.

*Correspondence: tangdian@fzu.edu.cn, mse_dongdh@ujn.edu.cn and kxie@fjirsm.ac.cn.

Tel/Fax: +86-591-63179173.

Abstract

The significant role of perovskite defect chemistry through A-site doping of strontium titanate with lanthanum for CO_2 electrolysis properties is demonstrated. Here we present a dual strategy of A-site deficiency and promoting adsorption/activation by making use of redox active dopants such as Mn/Cr linked to oxygen vacancies to facilitate CO_2 reduction at perovskite titanate cathode surfaces. Solid oxide electrolysers based on oxygen-excess $La_{0.2}Sr_{0.8}Ti_{0.9}Mn(Cr)_{0.1}O_{3+\delta}$, A-site deficient $(La_{0.2}Sr_{0.8})_{0.9}Ti_{0.9}Mn(Cr)_{0.1}O_{3-\delta}$ and undoped $La_{0.2}Sr_{0.8}Ti_{1.0}O_{3+\delta}$ cathodes are evaluated. *In situ* infrared spectroscopy reveals that the adsorbed and activated CO_2 adopts an intermediate chemical state between a carbon dioxide molecule and a carbonate ion. The double strategy leads to optimal performance being observed after 100 h of high-temperature operation and 3 redox cycles, suggesting a promising

cathode material for CO_2 electrolysis.

Introduction

Solid oxide electrolysers (SOEs) have been attracting great interest due to their high efficiency in converting electrical energy into chemical energy[1-2]. They can exploit available heat streams such as nuclear power plants or industrial waste heat to maximize electrical efficiency while both thermodynamic and kinetic advantages can be expected because of the high operating temperatures[3]. The oxide ion-conducting SOEs can directly electrolyse carbon dioxide into carbon monoxide and pure oxygen under external applied potentials. At the cathode, the CO_2 molecules are electrochemically reduced and split into CO while the generated O^{2-} ions are transported through the electrolyte membrane to the anode compartment where the pure O_2 gas is formed and released[2, 4].

Such materials have formed a starting point for SOE development and primarily include Ni/yttria-stabilized zirconia (Ni/YSZ) cermet for the cathode and (La,Sr)MnO_3 for the anode[5]. Recent studies have considered alternative materials to Ni/YSZ for the SOE cathode, and these have included the utilization of (La,Sr)$TiO_{3+\delta}$[6] and $La_{0.75}Sr_{0.25}Cr_{0.5}Mn_{0.5}O_3$[7] perovskites. A primary motivation for the investigation of alternative SOE cathode materials is the instability of Ni/YSZ to redox cycling, which in practice requires feeding a small quantity of protecting gas such as hydrogen or CO at the electrolysis cell cathode inlet in order to avoid the formation of NiO at low or zero electrolysis current density[8-9]. In contrast, oxide perovskites are generally stable to redox cycling and can therefore be operated without the requirement of protecting gas in the electrolysis cell cathode inlet. Furthermore, appropriate doping of the A/B-site of ABO_3 perovskites would allow properties to be tuned specifically to meet the demands of SOEs, such as operation under high temperature and strongly reducing environment.

La-doped strontium titanates exhibit favourable chemical, dimensional, redox, thermal and mechanical stability[10]. In addition, these perovskites demonstrate good electronic conductivity under reducing conditions due to the formation

of the Ti^{4+}/Ti^{3+} redox couple, which is particularly suitable for the reducing environment encountered at the electrolysis cell cathode[11]. Lattice defect formation is made possible by aliovalent doping of the A-site of $SrTiO_3$, for example, some of the divalent Sr^{2+} cations are substituted with trivalent La^{3+} cations. The defect chemistries considered here are oxygen-excess ($ABO_{3+\delta}$) and A-site deficiency ($A_{1-x}BO_3$). However, cathode performance for CO_2 electrolysis is still limited by insufficient electro-catalytic activity and the weak high-temperature chemical adsorption of reactants[12].

In oxide-ion-conducting SOEs, insufficient adsorption of CO_2 in cathode is always a limitation, which leads to the local starvation and then restricts electrolysis performances[13]. The linear CO_2 molecules in the absence of polarity are not easy to be chemically adsorbed and activated, especially at high temperatures. It is common to observe that the local starvation of CO_2 mainly leads to the large electrode polarizations and low current efficiencies for the electrolysis of CO_2 at high temperatures[14-16]. Currently preferred chemical adsorption of CO_2 on solid oxide materials is based on grafting a solid amine and producing an alkaline surface; however, the desorption temperature is normally below 500 ^oC which is far below the operation temperature of SOEs[17-20]. The defected sites with oxygen vacancies on the surface of solid oxide materials provide the promising possibilities for the chemical adsorption of CO_2 as these sites could act as host sites to accommodate the linear CO_2 molecules, which is expected to significantly extend the onset temperature of chemical desorption of CO_2 and benefit the cathode[21-22]. In addition, the chemically adsorbed CO_2 molecules are expected to be strongly activated on these vacancy-related defect sites and consequently favorable for electrochemical reduction at high temperatures.

In this work, the redox-active Mn/Cr with multi-oxidation states is introduced into the B-site of the oxygen excess $La_{0.2}Sr_{0.8}Ti_{1.0}O_{3+\delta}$ and A-site deficient titanates to create the oxygen vacancies both in the bulk and on the surface for the chemical adsorption of CO_2 molecules. The electrical properties and efficient electrochemical CO_2 splitting are then achieved in the active surface structures on titanate cathode. Direct CO_2 electrolysis is then investigated in the

oxide-ion-conducting SOEs at 800 ºC.

Experimental

Ceramic oxides including $La_{0.2}Sr_{0.8}Ti_{1.0}O_{3+\delta}$ (LST_{O+}), $La_{0.2}Sr_{0.8}Ti_{0.9}Cr_{0.1}O_{3+\delta}$ ($LSTC_{O+}$), $La_{0.2}Sr_{0.8}Ti_{0.9}Mn_{0.1}O_{3+\delta}$ ($LSTM_{O+}$), $(La_{0.2}Sr_{0.8})_{0.9}Ti_{0.9}Mn_{0.1}O_{3-\delta}$ ($LSTM_{A-}$), $(La_{0.2}Sr_{0.8})_{0.9}Ti_{0.9}Cr_{0.1}O_{3-\delta}$ ($LSTC_{A-}$), $(La_{0.8}Sr_{0.2})_{0.95}MnO_{3-\delta}$ (LSM) and $Ce_{0.8}Sm_{0.2}O_{2-\delta}$ (SDC) powders were synthesized using a solid-state reaction method performed in air[23-24].

The phase formations were confirmed by using X-ray diffraction (XRD, Cu Kα, Miniflex600, Rigaku Corporation, Japan) and the data were refined by using the General Structure Analysis System (GSAS) software[25]. The microstructure of the symmetric cells was investigated by scanning electron microscopy (SEM, SU-8010, JEOL Ltd, Japan). High-resolution transmission electron microscopy (HRTEM, Tecnai F20, FEI Ltd, USA) was also employed to investigate the microstructures of the samples. X-ray photoelectron spectroscopy (XPS, ESCALAB 250Xi, Thermo, USA) with monochromatized Al Kα at hv = 1486.6 eV was utilized to analyze the element states. The TGA tests of the samples were conducted on a thermal analyzer (STA449F3, Netzsch). All infrared spectra were collected with a resolution of 4 cm^{-1} and 64 scans by a Fourier transform infrared spectrometer (VERTEX 70, Bruker). The powder samples were first reduced in 5% H_2/Ar at 800 °C for 20 h and then treated in CO_2 at 450 °C for 1 h and the *in situ* IR test was subsequently performed. The electrical properties were examined by the DC four-terminal method. The conductivity was measured using an online multi-meter (Keithley 2000, digital multimeter, Keithley Instruments Inc., USA).

The electrolyte-supported symmetric cells with 0.5-mm-thick YSZ electrolyte and different titanate electrodes (1 cm^2) were assembled and treated at 1200 ºC for 3 h in air. The current collector of the silver paste (SS-8060, Xinluyi, China) was printed on both surfaces of the electrodes. Silver wire (0.2 mm in diameter) was used as the lead wire and attached to the Ag current collector using conductive adhesive (DAD87, Shanghai Research Institute for

Synthetic Resins, China) and treated at 550 °C for 30 min in air. The 0.5-mm-thick YSZ-supported single SOEs with titanate cathodes (1 cm^2) and LSM anode (1 cm^2) were assembled and treated at 1200 °C for 3 h in air. Electrochemical measurement of the cells was performed using an electrochemical station (IM6, Zahner, Germany) with a frequency range of 4 MHz to 100 mHz and a voltage perturbation of 10 mV. The gas flow was controlled with the mass flow meters (D08-3F, Sevenstar, China). The electrolysis cells were sealed into a homemade testing jig using ceramic paste (JD-767, Jiudian, China) for the electrochemical test. The electrolysis experiment was conducted by flowing 5% H_2/Ar at the flow rate of 50 mL min^{-1} for 1.5 h and then pure hydrogen at the flow rate of 50 mL min^{-1} was supplied to the cathode for 2.0 h at the operation temperature. After that, the cathode would be sufficiently reduced and activated. CO_2 electrolysis was subsequently performed using an electrochemical station at different applied voltages (1.4, 1.6 and 1.8 V) with pure CO_2 (50 mL min^{-1}) fed into the cathode. The CO production was analyzed by using an online gas chromatograph (GC2014, Shimazu, Japan) for the exhaust stream from the electrolysers at 800 °C.

Results and discussion

Different perovskite defect chemistries and their combinations such as oxygen excess, A-site deficiency and Mn/Cr doping have been investigated, seeking to optimize electrolysis cathode properties. XRD analysis confirms the synthesis of pure-phase perovskite powders. The patterns are shown in Fig. 1(a) and (b). All oxidized samples could be indexed assuming a cubic symmetry, with space group *Pm-3m*. As shown in Fig. 1(c) and (d), on reduction, a unit cell expansion is observed due to the reductions of Ti and Mn. This is because most of the Mn^{4+} (0.530 Å) and part of the Ti^{4+} (0.0.605 Å) have been reduced to Mn^{3+} (0.0.645 Å) and Ti^{3+} (0.670 Å). Due to the A-site deficiency, the perovskite structure is retained for the titanate phase, suggesting structural redox stability. The doping and reduction of Mn/Cr should be coupled with the creation of additional oxygen vacancies in the titanate, which in turn should facilitate CO_2 chemisorption. XPS furthermore confirms the presence of the reduced species Ti^{3+} and Mn^{3+} within

the reduced $LSTM_{A-}$, corroborating the XRD results. As shown in Fig. 2(a), only Ti^{4+} is observed in the oxidized $LSTM_{A-}$; however, part of the Ti^{4+} is chemically reduced into Ti^{3+} by treating the $LSTM_{A-}$ in a reducing atmosphere due to the peak shift[26-27]. The lower valence states of Ti^{3+}, $Mn^{4+/3+}$ are present in reduced samples while most of the element is at high oxidation state in the oxidized samples.

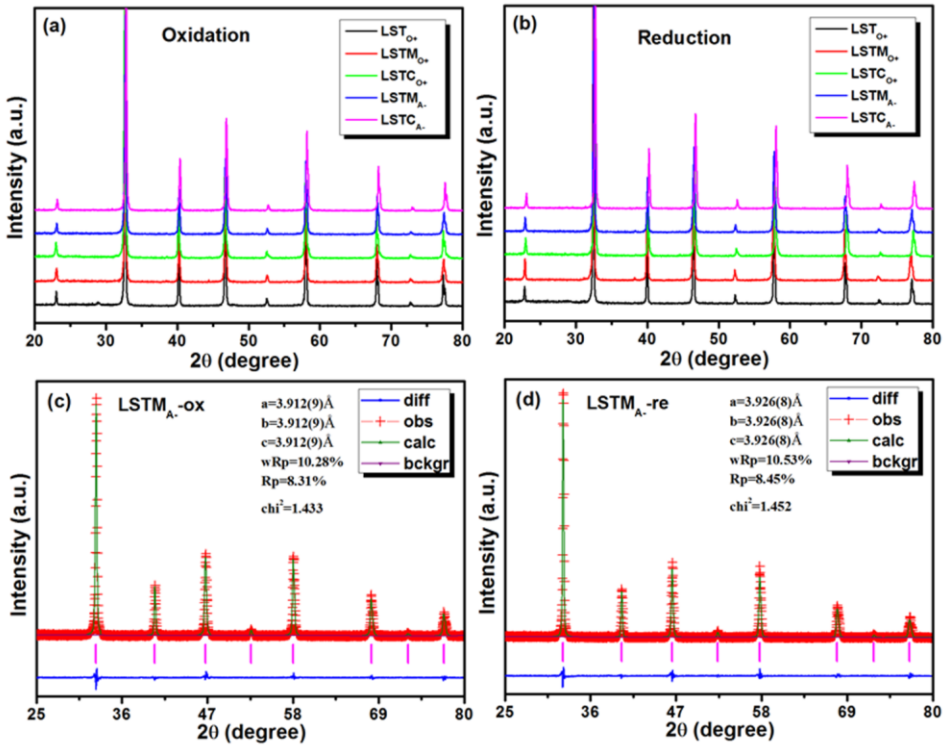

Fig. 1 XRD patterns of (a) oxidized and (b) reduced LST_{O+}, $LSTM_{O+}$, $LSTC_{O+}$, $LSTM_{A-}$ and $LSTC_{A-}$; XRD Rietveld refinement of (c) oxidized and (d) reduced $LSTM_{A-}$.

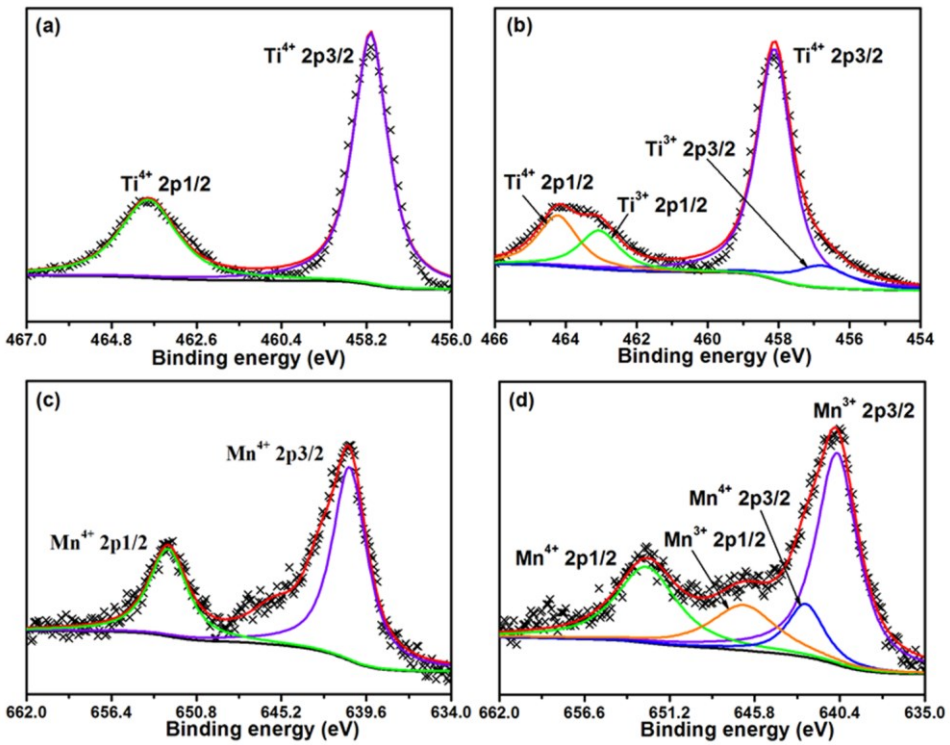

Fig. 2 XPS results for (a) Ti and (c) Mn in the oxidized $LSTM_{A-}$; (b) and (d) in the reduced $LSTM_{A-}$.

HRTEM analysis of the oxidized and reduced $LSTM_{A-}$ has revealed lattice spacing of 0.289 nm (110) and 0.278 nm (110), respectively, as shown in Fig. 3(a) and (b), consistent with the separation spacing determined by the XRD analysis. The differences of ionic radius may contribute to the changes of the lattice spacing. Thermogravimetric analysis on the various titanates, as shown in Fig. 4(a), suggests varying degrees of oxygen stoichiometry, depending on titanium substitution with Cr/Mn and A-site deficiency. Whereas LST_{O+} shows a change of 0.033 mol of oxygen upon oxidation/reduction, the Cr and Mn substituted stoichiometries release/absorb 0.041 and 0.057 mol of lattice oxygen for the $LSTC_{O+}$ and $LSTM_{O+}$, confirming the reducibility of the Mn and consequent formation of additional oxygen vacancies upon reduction. However, the Cr^{3+} in titanate lattice is less reducible that leads to similar oxygen

absorption for reduced LST_{O+} and $LSTC_{O+}$ samples. Strong reduction only produces partial transition of Cr^{3+} to Cr^{2+} as confirmed by the larger weight gains in TGA analysis. The weight changes increase even further upon A-site deficiency, suggesting that more oxygen vacancies of 0.060 and 0.073 mol are created for the $LSTC_{A-}$ and $LSTM_{A-}$, respectively. The varying oxygen contents and abilities to store and release lattice oxygen also manifest themselves in the oxide ionic conductivities of the titanates. The ion conductivity of sintered pellets is tested using the electron-blocking electrode method for the reduced states[28-29]. As shown in Fig. 4(b), reduced LST_{O+} has lowest ionic conductivity, reaching 9.6×10^{-4} S cm^{-1} at 800 °C. Upon substitution with Cr/Mn and consequently increasing oxygen vacancy concentration under reducing conditions, this increases by an order of magnitude to 6.1×10^{-3} and 6.4×10^{-3} S cm^{-1} for the $LSTC_{O+}$ and $LSTM_{O+}$, respectively. Introducing A-site deficiency causes an additional 20% increase to 7.4×10^{-3} and 8.2×10^{-3} S cm^{-1} for the $LSTC_{A-}$ and $LSTM_{A-}$ under identical conditions. It is expected that the oxygen vacancy defect sites are able to accommodate carbon dioxide molecules to exhibit the chemical adsorption behavior.

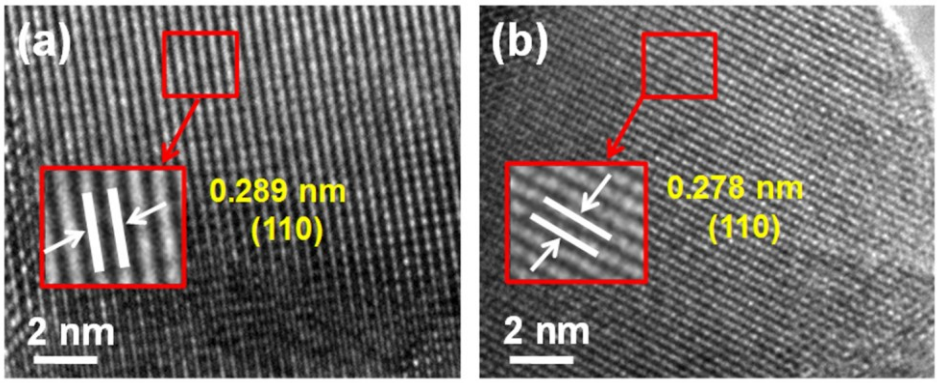

Fig. 3 HRTEM results for the (a) oxidized and (b) reduced $LSTM_{A-}$.

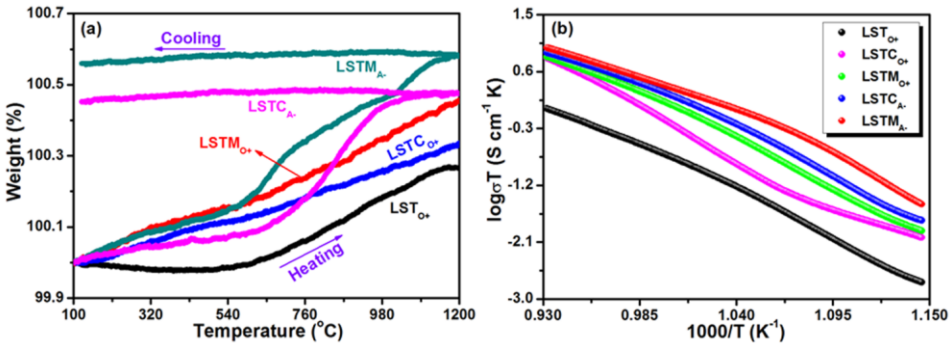

Fig. 4 (a) TGA tests of the reduced samples (800 °C for 20 h in 5% H_2/Ar) from 100 to 1200 °C in air; (b) The dependence of ionic conductivity on temperature of the reduced samples in 5% H_2/Ar.

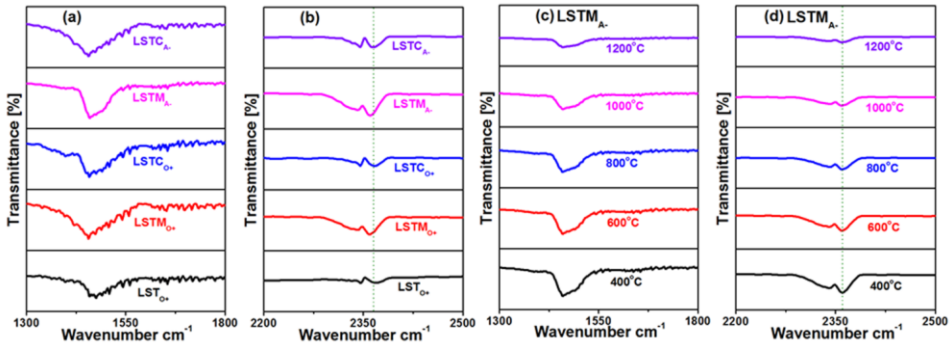

Fig. 5 (a) and (b) *in situ* IR spectra of CO_2 adsorbed on the reduced samples at room temperatures; (c) and (d) *in situ* IR spectra of CO_2 adsorbed on the reduced $LSTM_{A-}$ from 400 to 1200 °C.

The chemical adsorption of CO_2 molecules on reduced titanate samples was investigated by *in situ* IR spectroscopy. All samples with adsorbed CO_2 show absorption signals in two distinct IR bands at room temperature in Fig. 5(a) and (b), i.e. 2380 – 2300 cm^{-1}, which is associated with CO_2 molecules[30] on the sample surface and 1500 – 1430 cm^{-1}, which is typically observed for CO_3^{2-} [31]. The chemisorbed carbon dioxide on the titanate surface is therefore assumed to be intermediate between molecular CO_2 and carbonate ions. As expected from the concentration of oxygen ion vacancies, which should translate into an active oxide surface, the strongest IR absorption is observed for

the $LSTM_{A-}$ and $LSTC_{A-}$. To test the ability to adsorb CO_2 at elevated temperatures, $LSTM_{A-}$ was subjected to *in situ* IR tests between 400 and 1200 °C. As shown in Fig. 5(c) and (d), the strong chemical adsorption is still present even at 1200 °C, indicating the successful chemical CO_2 adsorption through control of oxygen vacancies and A-site deficiency. It is worth noting that both signals of carbonate and CO_2 molecules exist even at such high temperature, indicative of the presence of strong chemical adsorption of CO_2 on defected structure of titanate oxide.

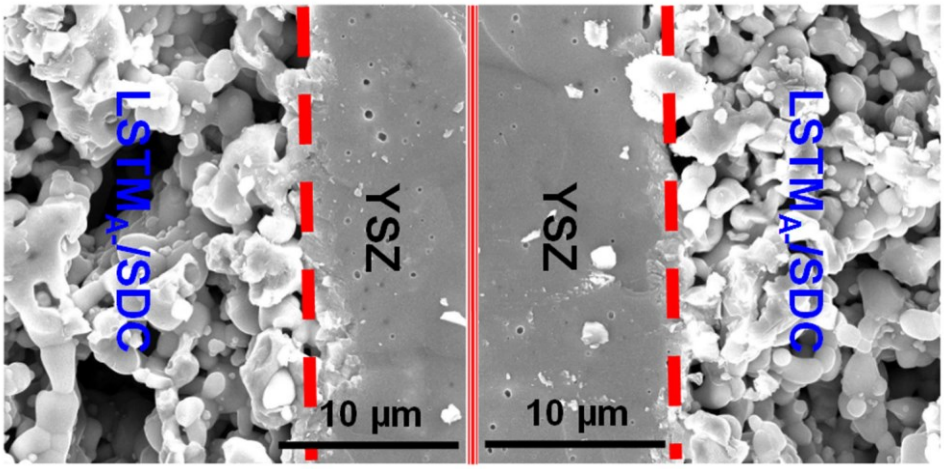

Fig. 6 Enlarged view of the electrode/electrolyte interfaces of the cross-sectional SEM images of the solid oxide symmetric cell with the cell configuration of $LSTM_{A-}$/SDC-YSZ-$LSTM_{A-}$/SDC.

Symmetrical electrolyser cell was fabricated, using composite titanate cathode with SDC. SDC is incorporated in the cathode since it has superior ionic conductivity and is expected to deliver oxygen ion transport while the titanate provides electronic conductivity. Cross section of the cell can be found in Fig. 6, showing porous electrodes and dense electrolytes. AC impedance was performed on the symmetrical cells to assess the electrode polarization behaviour under reducing conditions, with pH_2 ranging from 0.20 – 1.0 bar. For all titanates it was found that the series resistance, R_s mainly comes from ionic resistance of the YSZ electrolyte, was generally stable in a wide range of pH_2. In this case, the series resistance R_s has been set as 0 to compare the polarization resistance R_p. As shown in

Fig. 7(a), the R_p of the symmetric cell based on LST_{O+} decreases from 4.06 to 1.97 Ω cm^2 with increasing pH_2 ranging from 0.20 – 1.0 bar, which suggests that a stronger reducing atmosphere is beneficial for improving the electrode polarization. R_p for $LSTM_{O+}$ and $LSTC_{O+}$ decreases with increasing hydrogen concentration from 2.11 to 1.27 Ω cm^2 and 2.76 to 1.38 Ω cm^2, respectively, which is probably due to the enhanced charge transfer and species diffusion in titanate electrodes[21, 32]. In contrast, R_p for $LSTM_{A-}$ and $LSTC_{A-}$ significantly decreases from approximate 1.95 to 0.94 Ω cm^2 (pH_2: 0.20 – 1.0 bar) and 1.99 to 1.07 Ω cm^2, respectively, as the hydrogen concentration is increased, which again validates the enhancement of electrode activity by creation of oxygen vacancy in the lattice and A-site deficiency. The symmetrical cell results are summarized in Fig. 7(f), and $LSTM_{A-}$ and $LSTC_{A-}$ perform the best in pH_2 = 1.0 bar, which are lower than the other samples.

The direct electrolysis of pure CO_2 is studied in solid oxide electrolysers with 5 types of cathodes under a series of applied voltages ranging from 1.0 to 2.0 V at 800 °C. The open circuit voltage (OCV) of the cells was established by exposing the cathode and anode to pure H_2 and static air, respectively, and was found to reach 1.1 V, indicating good gas separation by the cells. Typical current – voltage (*I-V*) curves for the various cathode materials in direct CO_2 electrolysis mode are shown in Fig. 8(a). As expected from the previous findings, LST_{O+} shows the poorest performance, reaching a maximum current density of 0.25 A cm^{-2} at 2.0 V. Improved performance is observed for Mn/Cr substituted compositions, which can be attributed to enhanced CO_2 adsorption and activation at high temperatures. $LSTM_{O+}$ reaches a maximum current density of 0.52 A cm^{-2} at 2.0 V. The A-site deficiency shows a further improvement, with maximum current densities of 0.68 and 0.57 A cm^{-2} at 2.0 V for $LSTM_{A-}$ and $LSTC_{A-}$, respectively. As shown in Fig. 8(b), the stable current density with the $LSTM_{A-}$ cathode reaches 0.25, 0.40 and 0.54 A cm^{-2} at 1.4, 1.6 and 1.8 V, respectively. Similarly, the stable current density with $LSTC_{A-}$ cathode reaches 0.22, 0.32 and 0.46 A cm^{-2} at 1.4 – 1.8 V, respectively; these values are 1.8 – 2.2 times higher in contrast to the cell with the LST_{O+} cathode under the same conditions, which further indicates that the more oxygen vacancies and A-site

Commented [CFC1]:

Commented [CFC2R1]:

Commented [CFC3R1]: should add a reference here to support the statement "as expected from previous findings"

deficiency on electrode materials have played a significant role in promoting the process of CO_2 electrolysis.

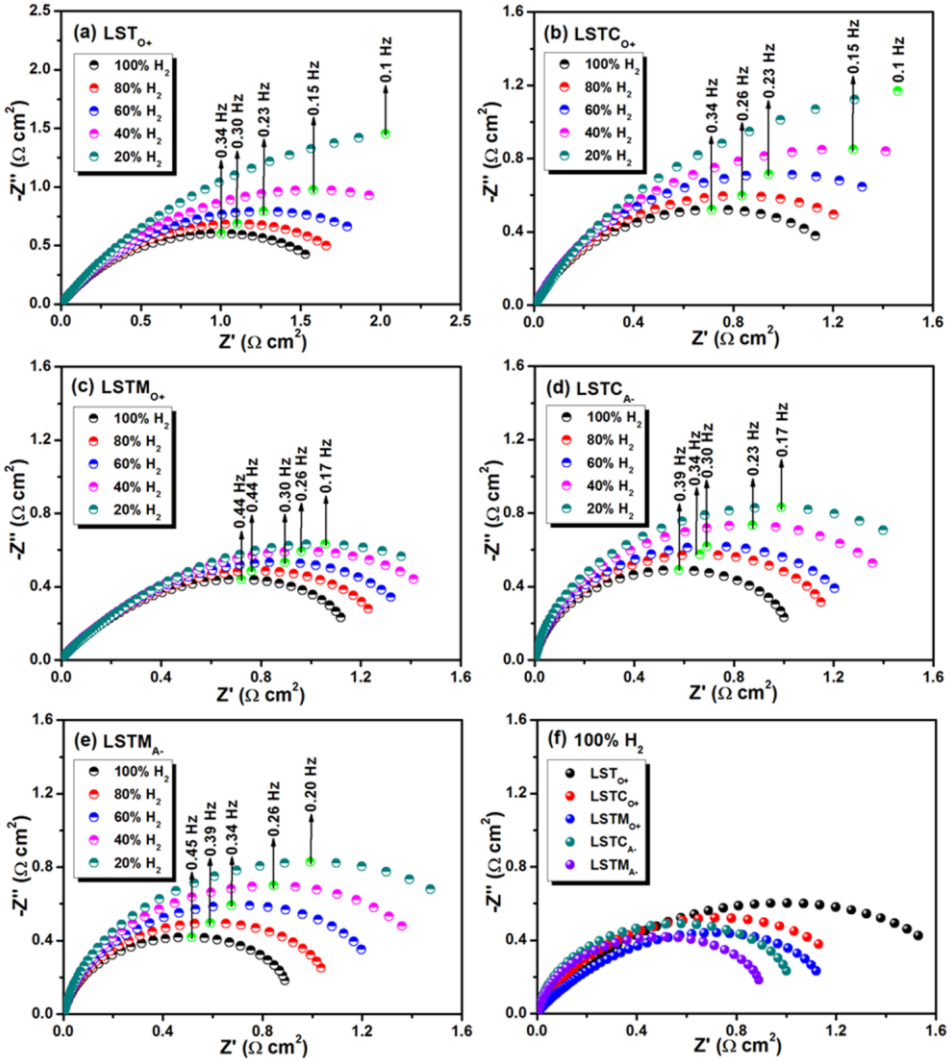

Fig. 7 AC impedance spectra of the symmetric cells for (a) LST_{O+}, (b) $LSTC_{O+}$, (c) $LSTM_{O+}$, (d) $LSTC_{A-}$ and (e) $LSTM_{A-}$ at various H_2 partial pressures at 800 °C; (f) AC impendence spectra of the symmetric cells with different electrodes in 100% H_2.

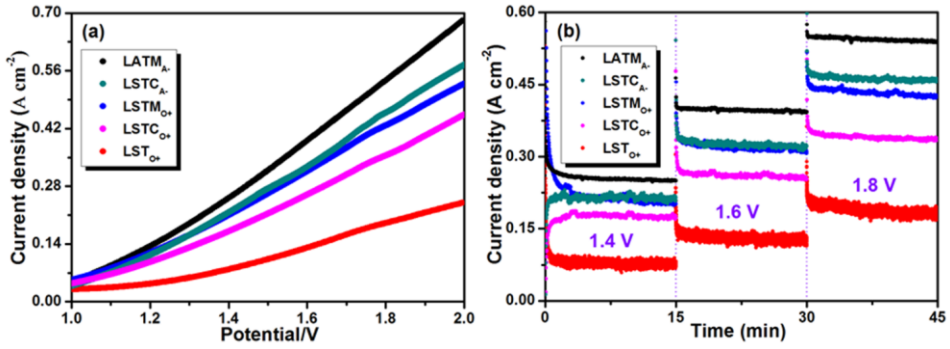

Fig. 8 (a) *I-V* curves of CO_2 electrolysis with different cathodes at 800 ºC; (b) Short-term performances of CO_2 electrolysis at different voltages.

To further understand the observed electrochemical performance in CO_2 electrolysis mode at 800 °C for the different cathode materials, impedance spectroscopy was carried out under a range of applied biases, i.e. 1.4 – 1.8 V. Similar trends are observed for all cathode materials in Fig. 9. It is observed that the R_s values are generally stable, whereas the R_p values obviously decrease as the applied voltages increase from 1.4 to 1.8 V. Increasing the voltage is expected to improve electrode polarization, following the improved kinetic process of the electrode. The applied voltage electrochemically reduces the composite cathode to enhance the conductivity and hence accordingly enhances the electrocatalytic activity of the composite electrode. At low frequency, the mass transfer especially for LST_{O+} cathode dominates the electrode process due to the dissociative adsorption, gas conversion and species transfer at the three-phase boundary (TPB). The R_p with LST_{O+} cathode improves from 1.43 to 0.92 Ω cm^2 at 1.4 to 1.8 V, respectively, suggesting improved gas conversion kinetics at high voltages. The R_p with $LSTM_{O+}$ cathode is reduced from 1.08 Ω cm^2 at 1.4 V to 0.64 Ω cm^2 at 1.8 V, because of the enhanced ionic conduction and chemical CO_2 adsorption. In contrast, The R_p with $LSTM_{A-}$ cathode significantly decreases to 0.82 Ω cm^2 at 1.4 V and is further reduced to 0.48 Ω cm^2 at 1.8 V, which demonstrates the A-site deficiency would further produce higher oxygen vacancy concentration that is beneficial to electrode activity enhancement[33]. Similar behavior has also been observed for $LSTC_{O+}$ and

$LSTC_{A-}$ cathodes. The catalytic activity of Mn itself in ABO_3 oxide is better than the Cr-doped sample, and the ionic conductivity of $LSTM_{A-}$ is higher than that of $LSTC_{A-}$. The above two points would accordingly deliver better performance for $LSTM_{A-}$ electrode even though $LSTC_{A-}$ has a higher oxygen vacancy concentration. The impedance spectra of different cathode materials at 1.8 V are summarized in Fig. 9(f).

Further evidence of these titanates' suitability to reduce CO_2 at the cathode comes from inspecting the rate of CO production as measured by gas chromatography and corresponding current efficiencies at different applied voltages, as shown in Fig. 10. The lower current efficiency may be because of the transport of impurity charge carriers in ceramic electrolyte especially the oxide ions and electrons. The maximum CO productions for the cell based on the $LSTM_{A-}$ and $LSTC_{A-}$ electrodes are approximately 3.66 and 3.03 mL min^{-1} cm^{-2}, respectively, which are 100-200% higher than 2.80, 2.27 and 1.12 mL min^{-1} cm^{-2} for $LSTM_{O+}$, $LSTC_{O+}$ and LST_{O+} electrodes at 1.8 V, respectively. In addition, the maximum current efficiencies with $LSTM_{A-}$ and $LSTC_{A-}$ cathodes are increased to 96.8% and 94.5% under the same conditions, again confirming the enhanced cathode activity with more oxygen vacancies. Results have been summarized in Table 1. In order to validate the long-term stability of the $LSTM_{A-}$ cathode, direct CO_2 electrolysis is performed at a fixed voltage of 1.4 V and 800 ºC for 100 h with pure CO_2 fed in the cathode. As shown in Fig. 10(c), the current density with $LSTM_{A-}$ cathode is stabilized at 0.25 A cm^{-2} with close to 100% current efficiency in the long-term test at high temperature, which confirms excellent stability of $LSTM_{A-}$ cathode with A-site deficiency and Mn-doping titanate for direct CO_2 electrolysis. To further investigate the cycling performance, the $LSTM_{A-}$ cathode is *in situ* repeatedly treated at 800 ºC in a 5% H_2/Ar or air and then tested for CO_2 splitting at 1.4 V for 1.5 h. The results show that the cell with $LSTM_{A-}$ cathode still demonstrates a comparable performance even after 3 redox cycles in Fig. 10(d). A-site deficiency together with B-site doping not only produces high temperature stability but also substantially enhances redox cycling performances for high temperature CO_2 electrolysis.

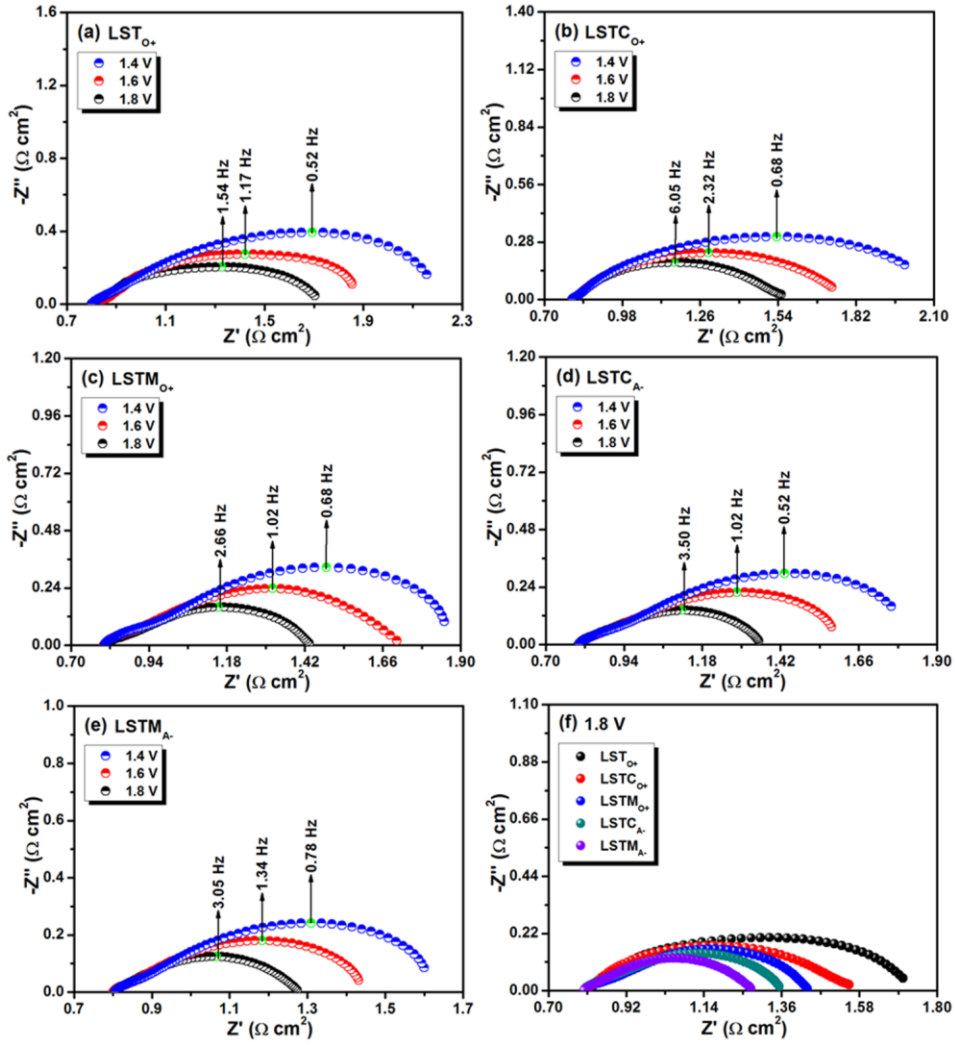

Fig. 9 *In situ* AC impedance spectra for electrolysers for different cathodes (a) LST_{O+}, (b) $LSTC_{O+}$, (c) $LSTM_{O+}$, (d) $LSTC_{A-}$ and (e) $LSTM_{A-}$ at various voltages; (f) *In situ* AC impendence spectra for electrolysers with different cathodes at 1.8 V with the flow of CO_2 at 800 ºC.

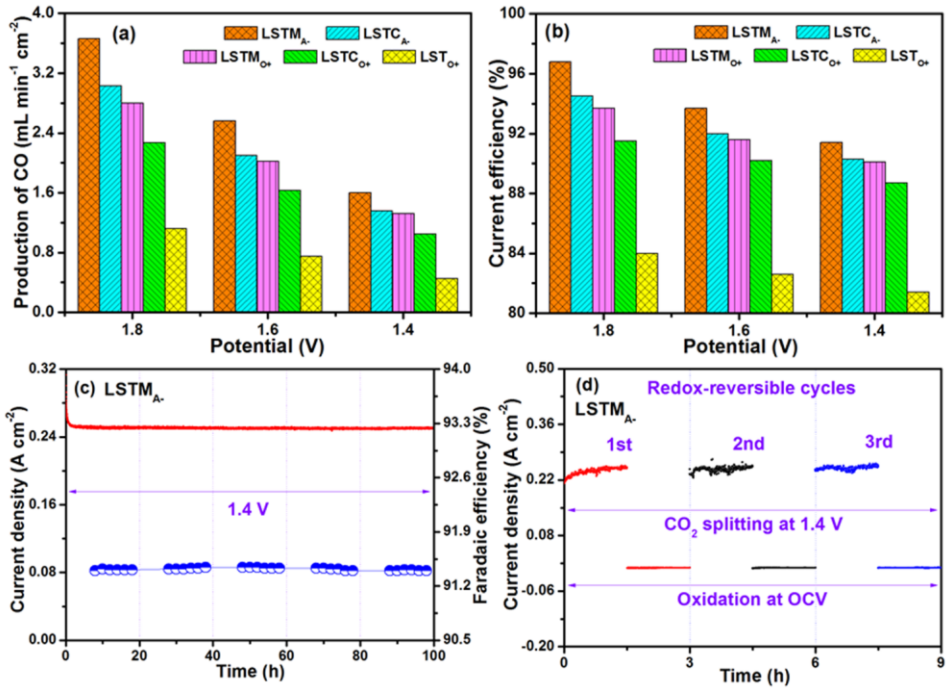

Fig. 10 (a) CO production and (b) current efficiency with different cathodes; (c) Long-term performance and current efficiency of the $LSTM_{A-}$ cathode with the flow of CO_2 at 800 °C; (d) Short-term performance of $LSTM_{A-}$ cathode after 3 redox cycles.

Table 1 The comparison of CO_2 electrolysis with different cathode at different applied voltages.

Cathode		Applied voltage (V)		
		1.4	1.6	1.8
LST_{O+}	CO production (mL min^{-1} cm^{-2})	0.45	0.75	1.12
	Current efficiency (%)	81.4	82.6	84.0
$LSTC_{O+}$	CO production (mL min^{-1} cm^{-2})	1.05	1.63	2.27
	Current efficiency (%)	88.7	90.2	91.5
$LSTM_{O+}$	CO production (mL min^{-1} cm^{-2})	1.32	2.02	2.80
	Current efficiency (%)	90.1	91.6	93.7
$LSTC_{A-}$	CO production (mL min^{-1} cm^{-2})	1.36	2.10	3.03
	Current efficiency (%)	90.3	92.0	94.5
$LSTM_{A-}$	CO production (mL min^{-1} cm^{-2})	1.60	2.56	3.66
	Current efficiency (%)	91.4	93.7	96.8

Conclusions

In summary, the remarkable chemical adsorption/activation of CO_2 at high temperature has been achieved by introducing more oxygen vacancies in Mn/Cr-doped and A-site deficient titanates. The ionic conductivities of A-site deficient and B-site doped titanates are greatly improved in reducing atmosphere. In addition, these titanates significantly enhance the cathode performances of CO_2 electrolysis and further exhibit high temperature stability as well as significant redox cycling ability. This study demonstrates that these titanates are promising candidates as alternative cathode materials in solid oxide electrolysers, providing the tools to develop next generation electrochemical devices for energy conversion and storage.

Acknowledgements

This work was supported by National Key Research and Development Program of China (2017YFA0700102), the Strategic Priority Research Program of the Chinese Academy of Sciences (XDB2003000), the Natural Science

Foundation of China (91845202 and 91545123), Natural Science Foundation of Fujian Province (2016J01275 and 2018J01088) and the U.S. National Science Foundation (1832809).

References

1. L. Ye, M. Zhang, P. Huang, G. Guo, M. Hong, C. Li, J. T. Irvine, and K. Xie, *Nat. Commun.*, 2017**, 8**, 14785.

2. X. Yue and J. T. S. Irvine, *J Electrochem. Soc.*, 2012**, 159**, F442-F448.

3. K. Xie, Y. Zhang, G. Meng and J. T. S. Irvine, *Energy Environ. Sci.*, 2011**, 4**, 2218-2222.

4. L. Zhang, S. Hu, X. Zhu and W. Yang, *Energy chem.*, 2017**, 195**, 7250-7254.

5. S. D. Ebbesen and M. Mogensen, *J. Power Sources*, 2009**, 193**, 349-358.

6. G. Tsekouras and J. T. S. Irvine, *J. Mater. Chem.*, 2011, **21**, 9367-9376.

7. S. Tao and J. T. S. Irvine, *Nat. Mater.*, 2003, **2**, 320.

8. R. Knibbe, M. L. Traulsen, A. Hauch, S. D. Ebbesen and M. Mogensen, *J. Electrochem. Soc.*, 2010, **157**, B1209-B1217.

9. P. Kim-Lohsoontorn and J. Bae, *J. Power Sources*, 2011, **196**, 7161-7168.

10. Y. Gan, Q. Qin, S. Chen, Y. Wang, D. Dong, K. Xie and Y. Wu, *J. Power Sources*, 2014, **245**, 245-255.

11. J. Lu, S. Li, S. Tao, T. Zhang and K. Xie, *Int. J. Hydrogen Energy*, 2017, **42**, 8197-8206.

12. L. Yang, K. Xie, L. Wu, Q. Qin, J. Zhang, Y. Zhang, T. Xie and Y. Wu, *Phys. Chem. Chem. Phys.*, 2014, **16**, 21417-21428.

13. M. Cassidy, D. J. Doherty, X. Yue and J. T. S. Irvine, *ECS Trans.*, 2015, **68**, 2047-2056.

14. X. Yue and J. T. S. Irvine, *Solid State Ionics*, 2012, **225**, 131-135.

15. C. Graves, S. D. Ebbesen and M. Mogensen, *Solid State Ionics*, 2011, **192**, 398-403.

16. Z. Zhan, W. Kobsiriphat, J. R. Wilson, M. Pillai, I. Kim and S. A. Barnett, *Energy Fuel.*, 2009, **23**, 3089-3096.

17. J. C. Hicks, J. H. Drese, D. J. Fauth, M. L. Gray and G. G. Qi, *J. Am. Chem. Soc.*, 2008, **130**, 2902-2903.

18. R. A. Khatri, S. S. C. Chuang, Y. Soong and M. M. Gray, *Energy Fuel.*, 2006, **20**, 1514-1520.

19. W. F. Schneider, *J Phys. Chem. B*, 2015, **108**, 273-282.

20. L. Ye, C. Pan, M. Zhang, C. Li, F. Chen, L. Gan and K. Xie, *ACS Appl. Mater. Inter.*, 2017, **9**, 25350-25357.

21. W. Qi, Y. Gan, D. Yin, Z. Li, G. Wu, K. Xie and Y. Wu, *J. Mater. Chem. A*, 2014, **2**, 6904-6915.

22. M. Nolan, *J. Phys. Chem. C*, 2016, **113**, 2425-2432.

23. J. Lu, C. Zhu, C. Pan, W. Lin, J. P. Lemmon, F. Chen, C. Li and K. Xie, *Sci. Adv.*, 2018, **4**, eaar5100.

24. S. Li, Q. Qin, K. Xie, Y. Wang and Y. Wu, *J. Mater. Chem. A*, 2013, **1**, 8984-8993.

25. S. Tao and J. T. S. Irvine, *Solid State Ionics*, 2008, **179**, 725-731.

26. M. Çopuroğlu, H. Sezen, R. L. Opila and S. Suzer, *ACS Appl. Mater. Inter.*, 2013, **5**, 5875-5881.

27. P. Cakir, R. Eloirdi, F. Huber, R. J. M. Konings and T. Gouder, *J. Phys. Chem. C*, 2014, **118**, 24497-24503.

28. X. Li, H. Zhao, F. Gao, Z. Zhu, N. Chen and W. Shen, *Solid State Ionics*, 2008, **179**, 1588-1592.

29. K. Shan and X. M. Guo, *Mater. Lett.*, 2013, **113**, 126-129.

30. M. C. Figueiredo, I. Ledezmayanez and M. T. M. Koper, *ACS Catal.*, 2016, **6**, 2382-2392.

31. W. Su, J. Zhang, Z. Feng, T. Chen, P. Ying and C. Li, *J. Phys. Chem. C*, 2008, **112**, 7710-7716.

32. Y. Li, G. Wu, R. Cong, Q. Zhou, Y. Wang, W. Doherty, K. Xie and Y. Wu, *J. Power Sources*, 2014, **253**, 349-359.

33. C. D. Savaniu and J. T. S. Irvine, *J. Mater. Chem.*, 2009, **19**, 8119-8128.